Optimisation of an elastomeric pre-buckled honeycomb helmet liner for advanced impact mitigation

Rhosslyn Adams[1] , **Shwe Soe**[2] **and Peter Theobald**[1,*]

[1] School of Engineering, Cardiff University, Cardiff, United Kingdom
[2] School of Engineering, University of the West of England, Bristol, United Kingdom

E-mail: TheobaldPS@Cardiff.ac.uk

CrossMark

Abstract

Advances in computational modelling now offer an efficient route to developing novel helmet liners that could exceed contemporary materials' performance. Furthermore, the rise of accessible additive manufacturing presents a viable route to achieving otherwise unobtainable material structures. This study leverages an established finite element-based approach to the optimisation of cellular structures for the loading conditions of a typical helmet impact. A novel elastomeric pre-buckled honeycomb structure is adopted and optimised, the performance of which is baselined relative to vinyl nitrile foam under direct and oblique loading conditions. Results demonstrate that a simplified optimisation strategy is scalable to represent the behaviour of a full helmet. Under oblique impact conditions, the optimised pre-buckled honeycomb liner exceeds the contemporary material performance when considering computed kinematic metrics head and rotational injury criterion, by up to 49.9% and 56.6%. Furthermore, when considering tissue-based severity metrics via finite element simulations of a human brain model, maximum principal strain and cumulative strain density measures are reduced by 14.9% and 66.7% when comparing the new material, to baseline.

(Some figures may appear in colour only in the online journal)

1. Introduction

Traumatic brain injury (TBI) is the most severe form of head injury and can arise from accidents within sports, crashes, or blasts, leading ultimately to disability or death [1]. For example, in snow sports, despite their lower incidence relative to knee and wrist injuries, head injuries present higher severity due to increased impact velocity [2]. It has been reported that of the 600 000 annual snow sport injuries in North America, 15%–20% involve head injuries [3]. Furthermore, death among participants under the age of 18, are primarily due to TBI (67%) [4]. Consequently, advanced protection within this sport, and many other helmeted sports, is of critical importance.

The use of a helmet is adopted to minimise the likelihood of sustaining a head injury—it is the most effective method for mitigating the risk of head injury. Conventionally, helmets are designed to protect the head against direct translational forces that give rise to injuries such as skull fracture [5, 6].

This is contrary to the well-established understanding that the main TBI mechanism is the exposure of rotational acceleration to the head, from oblique impacts [7–10]. Indeed, much effort has focussed on understanding the relationship between impact accelerations and head responses to improve the protection of head against impact loads [11, 12]. This has motivated the use of kinematic-based severity metrics [13, 14], as well as tissue-based metrics derived from finite element models of the human head to monitor impact exposure in helmeted impacts [15, 16]. Moreover, risk, location, and extent of structural damage for specific cases have been identified using finite element models [17–19]. Hence, there is an emerging consensus that emerging helmet technologies should be verified and protective helmet performance established using finite element head models [20].

Conventional helmet liners typically mitigate impact by being constructed from expanded polystyrene (EPS) or vinyl nitrile (VN) foam [21], with their energy absorbing properties defined by the density of the base material [22]. VN holds a unique advantage over EPS due to its ability to sustain several impacts without compromising its energy absorption capability [23, 24]. Accordingly, VN is highly desirable for protective devices that must respond effectively to consecutive impact events, like in snow sports, ice hockey and American football [25]. These foamed materials are, however, limited in terms of their ability to dissipate energy under shear, which occurs under oblique loading conditions [10]. Consequently, alternative materials are being sort that can offer high energy dissipation with low shear stiffness [26–28].

Advances in computational modelling now offers a route to developing novel helmet liners that could exceed contemporary materials' performance [29–31]. Furthermore, the rise of additive manufacturing presents a viable route to achieving otherwise unobtainable material structures [32–35]. Additively manufactured cellular structures have previously been evaluated with respect to the loading conditions of a helmet impact. For example, Soe *et al* numerically explored the use of an ordered lattice structure for impact mitigation within the volume of a helmet liner, demonstrating that tailorable energy absorption and thus impact mitigation can be achieved through structural changes [36]. This concept has since been expanded by Khosroshahi *et al*, who investigated the effect of lattice grading schemes and relative density on resultant head injury severity [37, 38]. Clough *et al* fabricated micro lattice impact attenuators, which afforded greater specific stiffness and densification strain, resulting in a reduction to peak acceleration under impact versus stochastically architectured foams [39]. The greater geometric freedom means architectured cellular structures hold a notable advantage over stochastic cellular structures. Hence, architectured cellular structures with tailorable mechanical properties represent a viable route to improving helmet liner performance.

The honeycomb is one such example of an architected cellular structure. This class of structure has been found in numerous applications such as aerospace, automotive and personal protective equipment [40], owing to their high relative energy
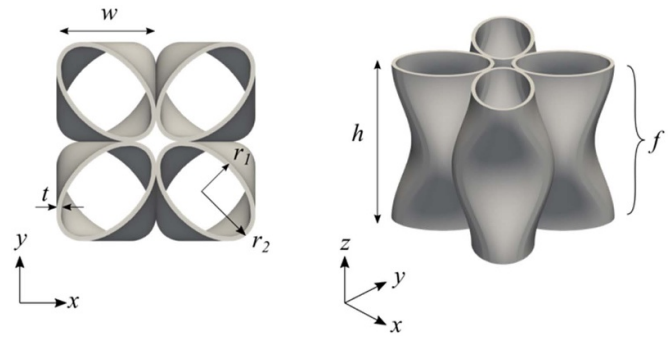
Figure 1. Proposed circular pre-buckled honeycomb topology described by parameters: cell size (w), wall thickness (t), height (h), minor radius (r_1), major radius (r_2) and number of folds (f).

dissipation that can be achieved at near constant stress [22]. The adoption of honeycomb type structures within helmet design improves user safety [41, 42]. For example, localised reinforcement [43, 44], exclusive use [45], or a hybrid combination of foam [46] and honeycombs provide superior performance relative to a monolithic equivalent. In all cases the principal mechanisms leveraged to mitigate the impact energy are plastic deformation and material fracture. These solutions are unsuitable for applications with potential for multiple (or consecutive) impacts, however, as the onset of permanent deformation will diminish helmet performance.

Several studies have indicated the suitability of elastomeric honeycomb-type structures for use in helmets, [47–49]. Our previous work identified a novel additively manufactured elastomeric circular pre-buckled honeycomb structure, which demonstrated excellent energy absorption capability during quasi-static and impact testing over successive loading cycles [50]. The topology (figure 1) was defined by structural parameters: cell size (w), wall thickness (t), height (h), minor radius (r_1) and major radius (r_2). The aspect ratio (e), used to describe the eccentricity of the circular cross-section was defined as the ratio of r_1 to r_2, whilst the fold (f) was based on a cosine function. The cosine wave approximates the natural symmetric crush mode of a straight walled tube. The implementation of this feature facilitates the ability to retain the stiffness-to-weight ratio of an axially compressed honeycomb, though removing the undesirable, inefficient peak stress prevalent in straight-walled designs.

In this study, we report on the same, pre-buckled honeycomb with variable out-of-plane behaviour, for use in head protection. Here we utilise a previously reported finite-element based strategy for the optimisation of cellular structures, subject to multi-impact loading conditions [51]. Whilst most studies focus on single-use conventional honeycombs derived from metals and rigid polymer, an elastomeric material definition is used which affords recoverability, suited for helmet applications requiring energy absorption across consecutive impacts. We optimise the structure before examining the performance under both direct and oblique impact loading conditions found in helmet certification tests. In addition

to kinematic-based injury metrics, a finite element model of a human head is used to identify the associated brain strain, to better assess the performance of the pre-buckled honeycomb relative to established materials in preventing TBI.

2. Materials and methods

In this section, the details of the pre-buckled honeycomb design are presented with respect to its structural parameters and the procedure for optimisation is outlined. Next, the full-scale finite element model of the honeycomb helmet, as well as the material properties of a contemporary liner material, VN, is reported. Further, the impact conditions to which the helmets will be subject to are presented. Lastly, the finite element head model used to establish TBI severity is detailed.

2.1. Honeycomb structure

The geometric parameters of the structure are defined to form a design window limiting density to <300 kgm^{-3}, a proposed upper bound when considered against comfort and wearability [52]. These values were: cell width ($w = 20.0$ mm), cell height ($h = 25.0$ mm), number of folds ($f = 1.0$), aspect ratio ($0.4 < e < 0.8$), and wall thickness ($0.6 < t < 1.5$ mm). Luvosint, a thermoplastic polyurethane utilised in additive manufacturing, was used as the base material of the honeycomb structure. Luvosint's behaviour has previously been reported [53].

2.2. Finite element-based optimisation

The pre-buckled honeycomb structure was optimised using a finite element-based strategy [51]. A periodic boundary condition (PBC) model was adopted to approximate the response to impact loading, avoiding the computational cost associated with successive simulations of a full-scale honeycomb helmet configuration. A 2×2 cell array was positioned between two analytically rigid plates, to approximate the anticipated crushing of the helmet liner between the shell and the head (figure 2(a)). This simplification has been used as it relates to previous validation studies [50], even though it is well established that the stiffness and topology of the shell has an influence on helmet behaviour. The lower plate was assigned an encastre boundary condition, with the upper assigned a point mass equivalent to BS EN 960 headform (size J) [54]. A pre-impact velocity of $v_z = 5.42$ ms^{-1} was adopted from the certification standard for alpine skiers and snowboarders helmet design (BS EN 1077) [55]. Global acceleration due to gravity, $a_g = 9.81$ ms^{-2}, was assigned to the entire model. As reported by figure 2(b), the perimeter nodes of the honeycomb array had a zero-displacement boundary condition, applied along the X and Y axes, whilst allowing displacement along the Z axis to facilitate deformation of the structure due to impact. The point mass of 4.7 kg was scaled to account for load distribution over a reduced portion of the area, calculated by normalising the honeycomb contact area relative to the anticipated impact

(a) Upper plate
Honeycomb
z
y
x
RP
a_g v_z
Lower plate

*(b)*
Infinite Structure
y
x
Nodal Boundary Conditions
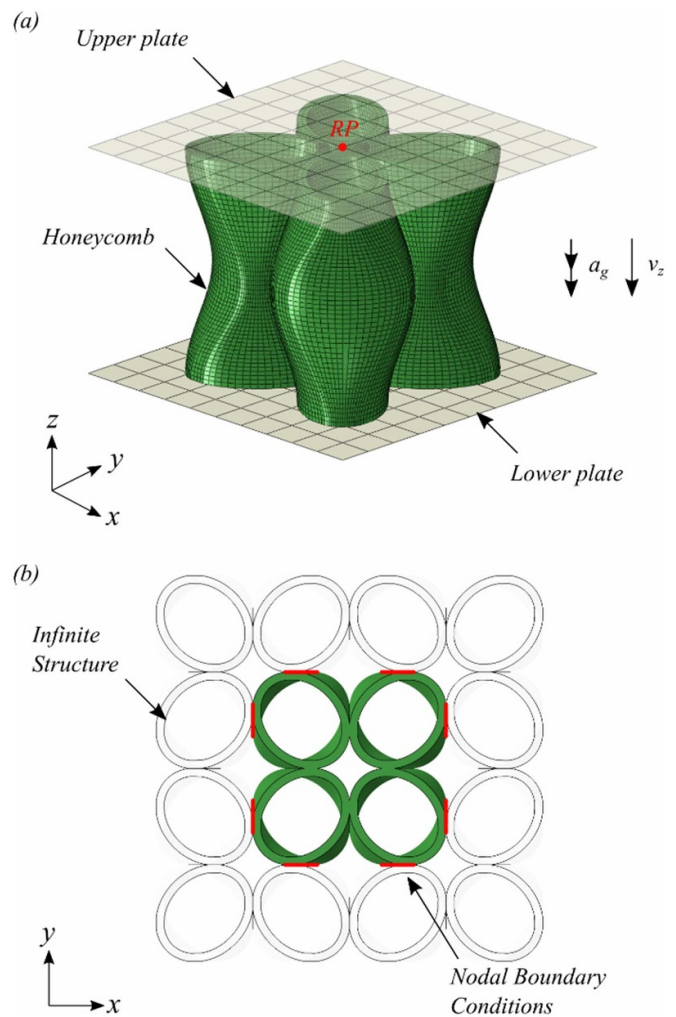
Figure 2. The finite element model of the pre-buckled honeycomb unit structure used during the optimisation strategy (a) comprised of four cells, positioned between two plates, (b) with nodal boundary conditions (red) to idealise an infinite structure.

area. The contact area of the PBC model, 1600 mm^2, was normalised by a circular contact area defined by the geometry of the helmet liner and headform interface of 9032 mm^2 [56]. Hence, the original point mass was assigned a scale factor of 0.18 yielding a mass of 0.845 kg.

The honeycomb mesh was constructed using eight-node brick elements with hexahedron shape type, reduced integration, and hourglass control (C3D8R). A mesh independence study was performed, with two elements across the wall thickness identified as a route to mitigate against shear locking. Elements had an average size 0.45 mm. A global friction value of 1.0 was used to emulate the anticipated friction that arises from self-contact of the elastomeric material.

Numerical optimisation was performed to identify honeycomb parameters that enabled effective impact mitigation, leveraging the efficacy of finite element simulations and the surrogate optimisation algorithm available in MATLAB's Optimisation Toolbox (MathWorks, United States). The optimisation procedure was run twice, subject to the limits
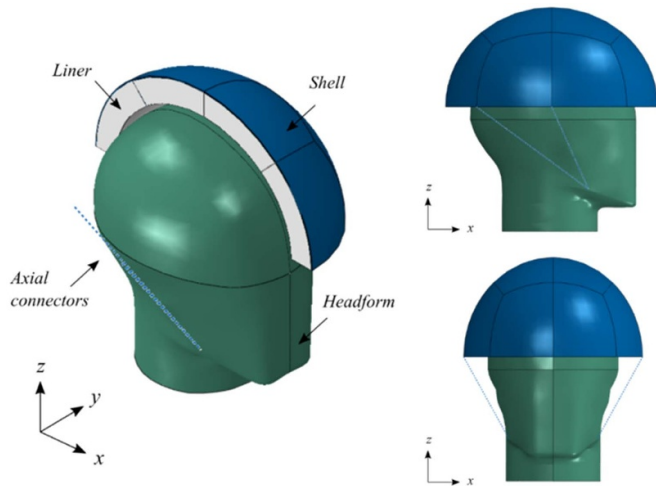
Figure 3. Construction of the finite element model including liner, shell, headform and retention strap (modelled as an axial connector).

Figure 4. Mapped meshing of honeycomb unit cells into a hexahedral guide mesh used to inform the honeycomb liner for the helmet finite element model.

described in section 2.1, each using 75 iterations. Firstly, the objective function was set to peak translational acceleration (PTA) compared to a critical value of 250 g, which is the maximum allowable value under the requirements of the helmet certification standard BS EN 1077. Secondly, the objective function was set to a head injury criterion (HIC) (refer to equation (1) threshold of 1574, which is equivalent to an abbreviated injury score of 4.

2.3. Complete helmet finite element model

The Abaqus explicit solver was used to simulate a helmeted headform impact, using finite element analysis. The model included the helmet shell and liner, anvil and headform (figure 3). The BS EN 960 headform (size J) was modelled, approximated as a surface, and considered analytically rigid, as it is several orders of magnitude stiffer than the helmet. The surface was meshed using a 3-node shell surface element with tetrahedral shape type. A point mass of 4.7 kg was applied at a reference point equivalent to the headform centre of gravity [35], and equivalent moments of inertia applied [57].

The helmet shell was approximated to a half-ellipsoid with principal radii, $r_{xs} = 135.0$ mm, $r_{ys} = 120.0$ mm, and $r_{zs} = 125.0$ mm. Shell thickness was $t_s = 1.0$ mm and modelled using linear brick elements, with reduced integration and hourglass control options. A mesh independence study was performed, with two elements across the wall thickness reporting stabilised results. Elements had an average size of 0.45 mm. Elements were assigned a linear elastic material model with a Young's modulus of $E = 7250.0$ MPa, Poisson ratio $\nu = 0.3$ and density $\rho = 1200$ kgm^{-3}, equivalent to the material properties of polycarbonate [58]. The shell-anvil surface interaction varied between the impact conditions; therefore, two coefficient of friction values were used. For direct impacts, $\mu_{\text{direct}} = 0.2$, whilst for oblique conditions, $\mu_{\text{oblique}} = 0.5$ [59]. For the headform helmet interface, a coefficient of friction value of 0.16 [60]. The retention strap was modelled as an elastic axial connector element, as per previous investigations
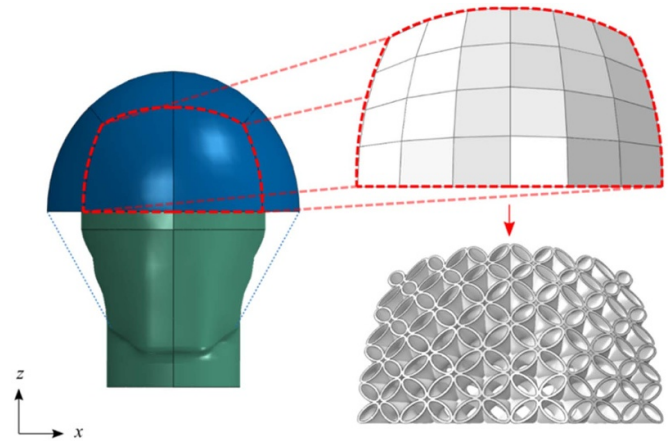
[61], which connects a reference node on the head from the chin surface to four points on the helmet. The axial load in the connector element corresponded to tensile behaviour of the retention strap, which produced a primary linear elastic behaviour.

An in-house mapped meshing system written in Python (Python 3.7) was used to construct a honeycomb liner, which adopted the conformal design envelope of a helmet. This leveraged a guide hexahedral mesh to propagate honeycomb unit cells and was approximated to a half ellipsoid shape, with principal radii, $r_{xl} = 110.0$ mm, $r_{yl} = 95.0$ mm and $r_{zl} = 100.0$ mm and a thickness of 25.0 mm. A global seed was assigned that yielded an element size of 40 mm, equivalent to twice the unit cell width used in the optimisation. The guide mesh informed the position, orientation, and scale of each unit cell (figure 4). The generated mesh was then imported into Abaqus, resulting in a curved section of honeycomb liner with the structural parameters established through the previously discussed optimisation process.

A computational elastomeric foam helmet liner was developed, to compare the pre-buckled honeycomb performance with a representative commercial material. The liner was modelled using linear brick elements with reduced integration and hourglass control options. At least 10 elements, with an average size of 1.85 mm, were meshed through the thickness to prevent shear locking. VN's strain-rate dependant mechanical behaviour for two densities (125 kgm^{-3} and 183 kgm^{-3}) was obtained from the literature, to calibrate a numerical material model [24]. The foam liner elements were modelled as a hyperelastic material, using the Hyperfoam model available in the Abaqus material library [62]. A 3 term ($N = 3$) polynomial was used with Poisson's ratio set to 0. Figure 5 illustrates the calibrated material model relative to the literature data.

2.4. Impact conditions

The helmeted headform was subject to direct and oblique impact loading. Direct impact testing onto a flat anvil was
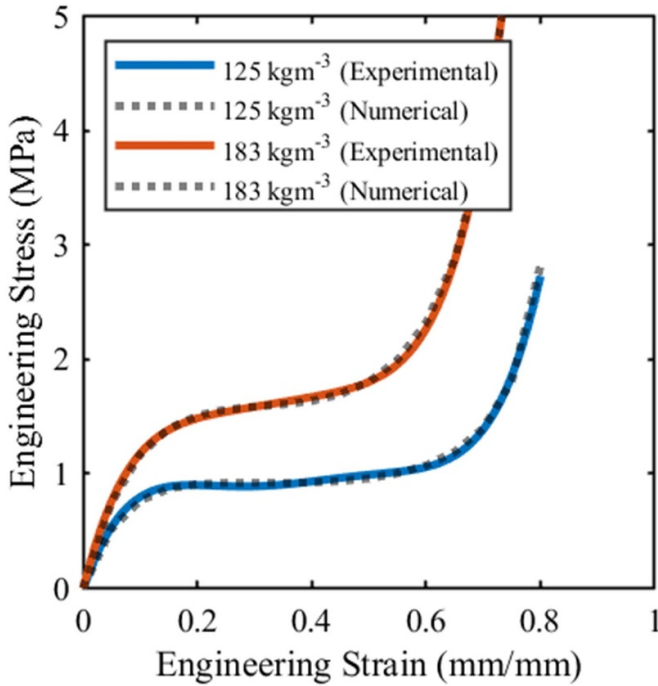
Figure 5. Comparison of compressive engineering stress and strain for the calibrated material model to experimental data for vinyl nitrile foam with density of 125 kgm^{-3} and 183 kgm^{-3}.

undertaken in accordance with shock absorption test method of EN 1077 (figure 6), with the helmeted headform given a 5.42 ms^{-1} initial velocity. Additionally, oblique impacts onto a 45° inclined flat anvil were performed in accordance with typical lab-based testing [63], with the helmeted headform given a 6.3 ms^{-1} initial velocity. Simulations were performed for 15 ms and components of translational and rotational acceleration, as well as translation and rotational velocity, were recorded from the headform centre of gravity.

To identify the resultant of severity of each impact and identify the performance of each helmet configuration, kinematic-based injury metrics were calculated using the translational and resultant acceleration. HIC [64], rotational injury criterion (RIC), and brain injury criterion (BrIC) [65] were calculated using equations (1)–(3)

$$\mathrm{HIC} = \max \left[\frac{1}{t_2 - t_2} \int_{t_1}^{t_2} a(t)\, \mathrm{d}t \right]^{2.5} (t_2 - t_1) \quad (1)$$

where a(t) is the resultant translational acceleration time history recorded from the centre of gravity of the headform. The time interval, $t_2 - t_1$, was chosen such that value of HIC was maximised

$$\mathrm{RIC} = \max \left[\frac{1}{t_2 - t_2} \int_{t_1}^{t_2} \alpha(t)\, \mathrm{d}t \right]^{2.5} (t_2 - t_1) \quad (2)$$
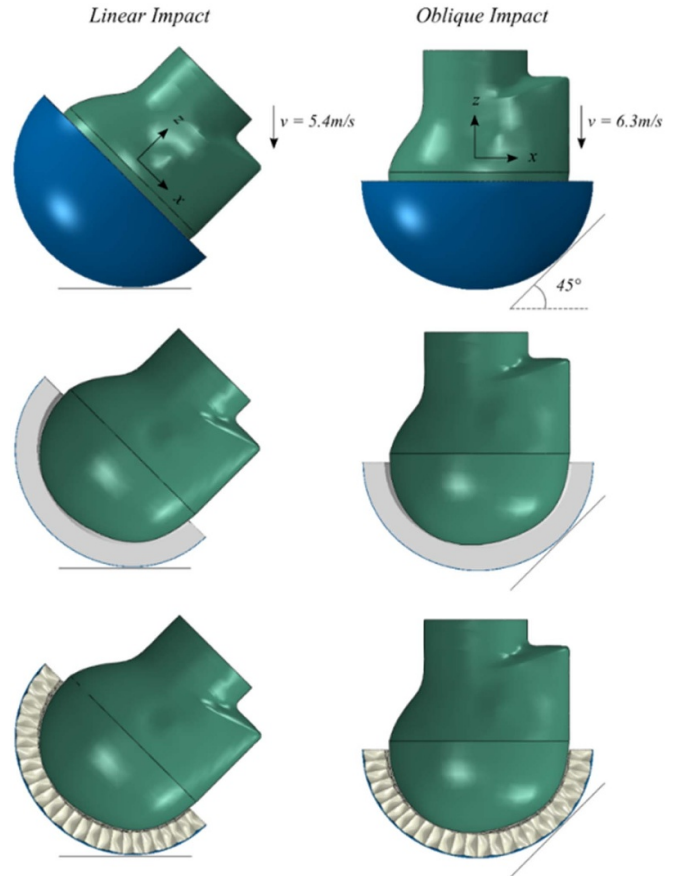
Figure 6. Orientation and conditions of direct and oblique impacts for foam and honeycomb liner helmets.

where α is the resultant rotational acceleration time history recorded from the centre of gravity

$$\mathrm{BrIC} = \sqrt{ \left(\frac{\omega_{x-\max}}{\omega_{xC}} \right)^2 + \left(\frac{\omega_{y-\max}}{\omega_{yC}} \right)^2 + \left(\frac{\omega_{z-\max}}{\omega_{zC}} \right)^2 } \quad (3)$$

where $\omega_{x-\max}$, $\omega_{y-\max}$ and $\omega_{z-\max}$ are the maximum rotational velocity about *X*, *Y* and *Z* axes respectively. ω_{xC}, ω_{yC}, and ω_{zC} are the critical angular velocity in their respective directions with values of 66.25, 56.45 and 42.87 rad s^{-1} respectively [65].

2.5. TBI assessment

Helmet efficacy was also assessed by estimating the relative brain strains developed during the above impacts, using the University College Dublin Brain Trauma Model [60, 66, 67]. The components of translational and rotational acceleration recorded during the helmeted headform impacts were used as the input to a node positioned at the model centre of gravity (figure 7).

Abaqus enabled the calculation of maximum principal strain (MPS) and volume fraction of elements, cumulative strain damage measure (CSDM), with an MPS exceeding a predefined strain threshold of 0.25. For the computation of
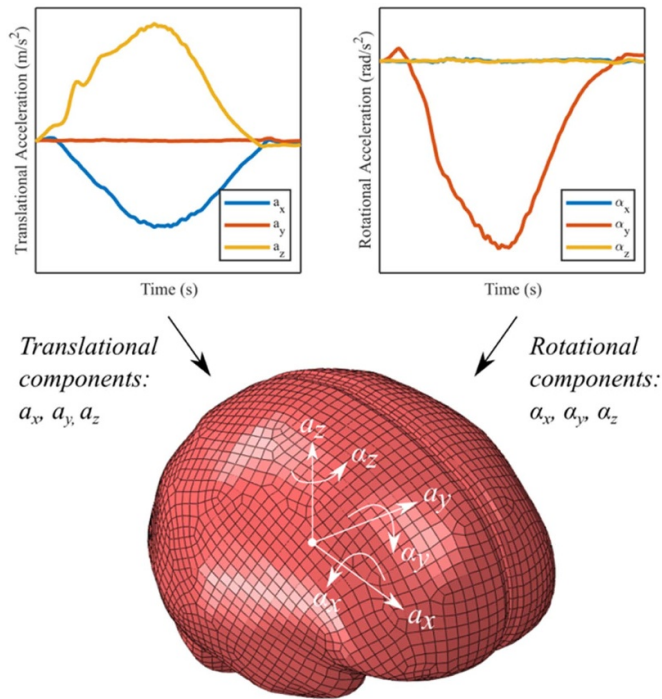
Figure 7. Annotated finite element head model with components of translational and rotational acceleration depicted as inputs to the model.

MPS, the 95th percentile value was adopted to mitigate against spurious results that arise from single elements. Analysis was restricted to the cerebrum, as per previous studies [60].

3. Results

### 3.1. Finite element-based optimisation

Finite element-based optimisation was undertaken to identify the optimal configuration of the honeycomb structure subject to the two objective functions. Figures 8(a) and (b) reports the variation in the objective function, peak translational acceleration, and HIC, for each evaluation.

In both cases, the optimisation procedure successfully satisfied the objective function. The optimal structures are hereafter identified as PTA$_{opt}$ and HIC$_{opt}$, to denote the objective function used to run the optimisation. For the PTA$_{opt}$ structure, the recorded PTA was 136.5 g and the calculated HIC was 960.7, whilst for the HIC$_{opt}$ structure, the recorded PTA was 165.9 g and the calculated HIC was 913.4. The structural and performance parameters of the optimal structures are reported in table 1.

3.2. Optimisation predictive efficacy

The honeycomb structures, identified through the optimisation procedure, were propagated within the volume of a helmet liner and subject to impact loading.

Both helmet liner configurations satisfy the design standard threshold. The PTA$_{opt}$ presents marginally higher acceleration during the loading of the helmet liner when compared to
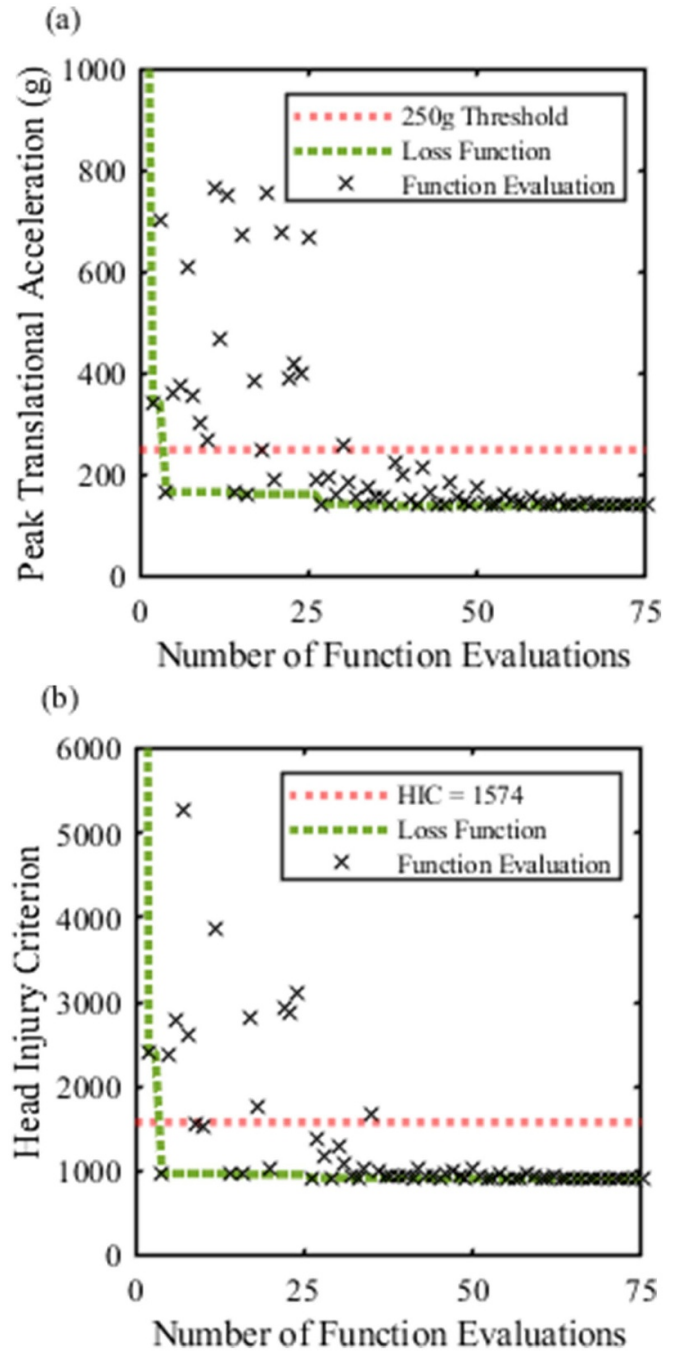
Figure 8. The variation in the objective function for peak translational acceleration (a) and head injury (b), relative to increasing optimisation iteration and a maximum allowable threshold value. Additionally, the loss function, defined as the minimised objective function computed per iteration, is reported.

HIC$_{opt}$, up until the point of peak acceleration where PTA is greatest for HIC$_{opt}$. The reported duration of each event was 12.5 ms and 13.7 ms, whilst HIC was calculated as 1162.2 and 1012.6 Percentage difference is reported for both PTA and HIC and is used to assess the predictive capacity of the proposed optimisation sequence. Generally, both PTA and HIC are underreported by the optimisation sequence. For PTA$_{opt}$, the relative difference was 35.2% and 20.9% for PTA and HIC,

Table 1. Structural and performance parameters of the optimal honeycomb configurations of each objective function.

Objective Function	Structural Parameters					Performance Parameters	
	w (mm)	t (mm)	e (-)	f (-)	ρ (kgm^{-3})	PTA (g)	HIC
PTA	20.0	1.62	0.60	1	276.9	136.5	960.7
HIC	20.0	1.11	0.80	1	198.0	165.9	913.4
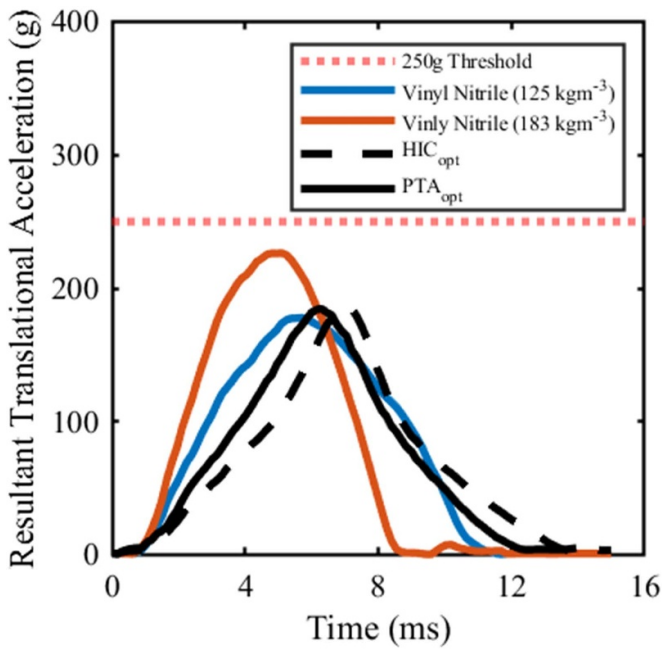
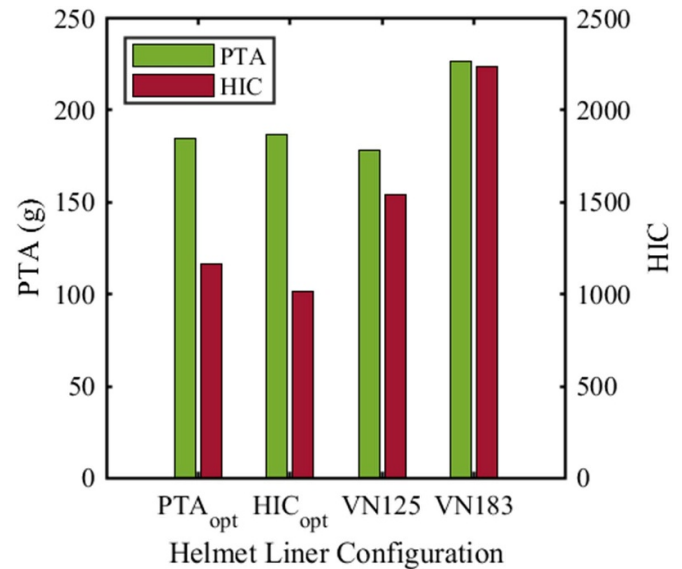**Figure 9.** Comparison of translational acceleration subject to direct impact conditions.

Figure 10. Comparison of severity metrics, peak translational acceleration, and head injury criterion, subject to direct impact conditions.

respectively. Comparatively, the relative difference reported for HIC$_{opt}$ was less than that of PTA$_{opt}$, where values of 12.7% and 10.9% were reported.

3.3. Liner impact performance

This section describes the liner impact performance of the optimised structures relative to an established helmet liner material, VN, under direct and oblique conditions using kinematic based injury metrics. The plots describe the helmet decelerating on impact (see 2.4 for inbound velocities), formatting consistent with the wider sector. For more information relating the kinematic data for each impact refer to the appendix A1.

3.3.1. Direct impact kinematic-based metrics.
The honeycomb structures were compared against VN foam to assess the potential to replace it as a helmet liner material. Figure 9 reports the resultant translational acceleration exposed to the headform during each impact under direct conditions. Furthermore, figure 10 reports a comparison of translational severity metrics PTA and HIC.

Comparison to VN foam demonstrates that both grades of material, 125 kgm^{-3} and 183 kgm^{-3}, hereafter referred to

as VN125 and VN183 respectively, can satisfy the requirements of the design standard (PTA $\leqslant$ 250 g). The profile of the acceleration curves for each report notably different behaviours. During the loading of the liner, values for translational acceleration exceed that of the honeycomb liners. Furthermore, at all points during loading, the value of translational acceleration for VN183 foams exceeds that of VN125. Peaks in acceleration are observed at 5.1 ms and 5.9 ms where the values for PTA are 226.5 g and 177.9 g for VN183 and VN125, respectively. The calculated HIC for VN183 exceeds that of the imposed threshold (HIC $\leqslant$ 1574) by 42.2%, whilst the HIC value for VN125 was 2.1% less than the threshold.

The minimum value for PTA, as recorded during the impact of VN125, was 177.9 g which is 3.8% and 5.1% less than that of the values recorded during the impacts of PTA$_{opt}$ and HIC$_{opt}$, respectively. When comparing HIC values, however, a more notable difference in performance is observed. The minimum value for HIC, as recorded again during the impact of VN125, was 1540 which is 24.5% and 34% greater than the values calculated during the impacts of PTA$_{opt}$ and HIC$_{opt}$, respectively.

3.3.2. Oblique impact kinematic-based metrics.
Figures 11(a) and (b) reports the resultant translational and rotational acceleration exposed to the headform during
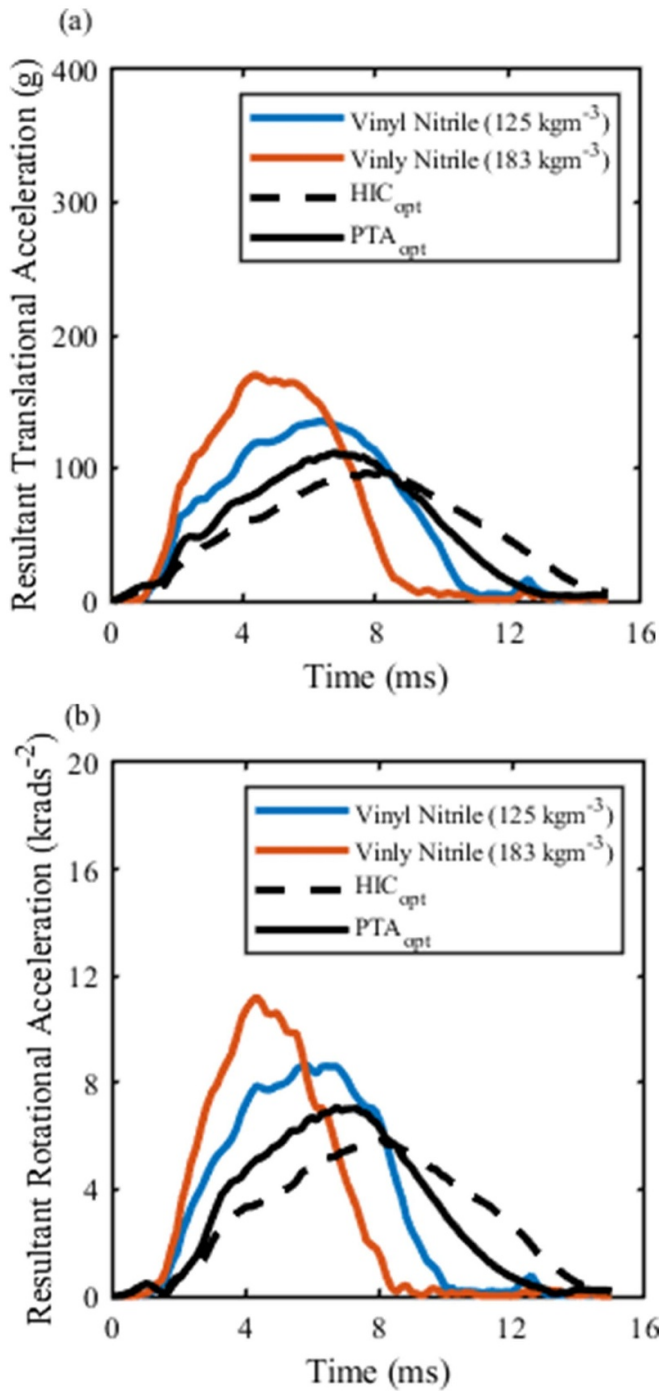
Figure 11. Comparison of translational (a) and rotational acceleration (b) subject to oblique impact conditions.

Figure 12. Comparison of kinematic based severity metrics, peak translational acceleration, and head injury criterion (a), peak rotational acceleration and rotational injury criterion (b), and (c) peak rotational velocity and brain injury criterion, subject to oblique impact conditions.

each impact. Furthermore, figures 12(a) and (b) reports a comparison of severity metrics PTA, PRA, HIC, RIC, PRA and BrIC.

Figure 11(a) shows that both liners with the pre-buckled honeycomb structure yield reductions in translational acceleration when compared to the foam liners. The profile of each translational acceleration curve reports notably different behaviour. During loading, up until the point of densification, values for translational acceleration of the foam liners exceed that of the pre-buckled honeycomb liners. Peaks in

translational acceleration are observed at 6.3 ms and 4.3 ms for VN125 and VN183, respectively, where the values for PTA are 135.1 g and 170.1 g. In comparison, the peaks in

translational acceleration for PTA$_{opt}$ and HIC$_{opt}$ are observed at 6.8 ms and 7.7 ms, respectively. At these points, the values for PTA are 111.7 g and 96.2 g, representing a relative reduction of 17.3% and 28.8% percent when compared to best performing foam (VN125). The impact duration recorded demonstrates a direct relationship to the HIC values calculated (figure 12(a)). For VN125 and VN183, the impact duration was 11.3 ms and 9.9 ms, whilst the HIC values were 847.4 and 1207.7. Similarly, for PTA$_{opt}$ and HIC$_{opt}$ the impact duration was 12.9 ms and 15 ms, whilst the HIC values were 529.8 and 424.8. Comparatively, this represents a reduction of 37.5% and 49.9%

Figure 11(b) shows that both liners with the pre-buckled honeycomb structure yield reductions in rotational acceleration when compared to the foam liners. The profile of each rotational acceleration curve reports notably different behaviour. During loading, values for rotational acceleration of the foam liners exceed that of the pre-buckled honeycomb liners. Peaks in rotational acceleration are observed at 5.9 ms and 4.4 ms for VN125 and VN183, respectively, where the values for PRA are 8.7 krads^{-2} and 11.2 krads^{-2}. In comparison, the peaks in rotational acceleration for PTA$_{opt}$ and HIC$_{opt}$ are observed at 6.8 ms and 8.1 ms, which are co-located with the peaks of translational acceleration. At these points, the values for PRA are 7.1 krads^{-2} and 5.8 krads^{-2}, representing a relative reduction of 18.4% and 33.3% percent when compared to the best performing foam (VN125). The impact duration recorded demonstrates a direct relationship to the RIC values calculated (figure 12(b)). For VN125 and VN183, the impact duration was 11.3 ms and 9.9 ms, whilst the RIC values were 25.2 × 10^6 and 30.2 × 10^6. Similarly, for PTA$_{opt}$ and HIC$_{opt}$ the impact duration was 12.9 ms and 15 ms, whilst the RIC values were 15.5 × 10^6 and 11.1 × 10^6. Comparatively, this represents a reduction of 38.3% and 56.6%.

Figure 12(c) reports severity metrics associated with rotational velocity. Peak rotational velocity (PRV) for VN125 and VN183, respectively, were reported as 44.7 rad s^{-1} and 47.3 rad s^{-1}, equivalent to a BrIC of 0.79 and 0.84. PTA$_{opt}$ and HIC$_{opt}$ pre-buckled honeycombs reported a PRV of 43.9 rad s^{-1} and 43.3 rad s^{-1} respectively, equivalent to a BrIC of 0.76 and 0.78. Comparatively, this represents a reduction in PRV and BrIC of 2.9%/

3.4. TBI assessment

This section describes the head injury mitigation efficacy of the optimised structures relative to VN under direct and oblique conditions, using a finite helmet head model to calculate tissue-based injury metrics.

Figure 13(a) reports the MPS$_{95th}$ and CSDM$_{0.25}$ for the direct impact conditions reported in figure 9. The values of MPS$_{95th}$ reported for foam liner configurations exceed the values reported for the honeycomb liner configurations. For VN125 and VN183, the MPS$_{95th}$ was 0.116 and 0.155 respectively. In comparison, the MPS$_{95th}$ for PTA$_{opt}$ and HIC$_{opt}$ were
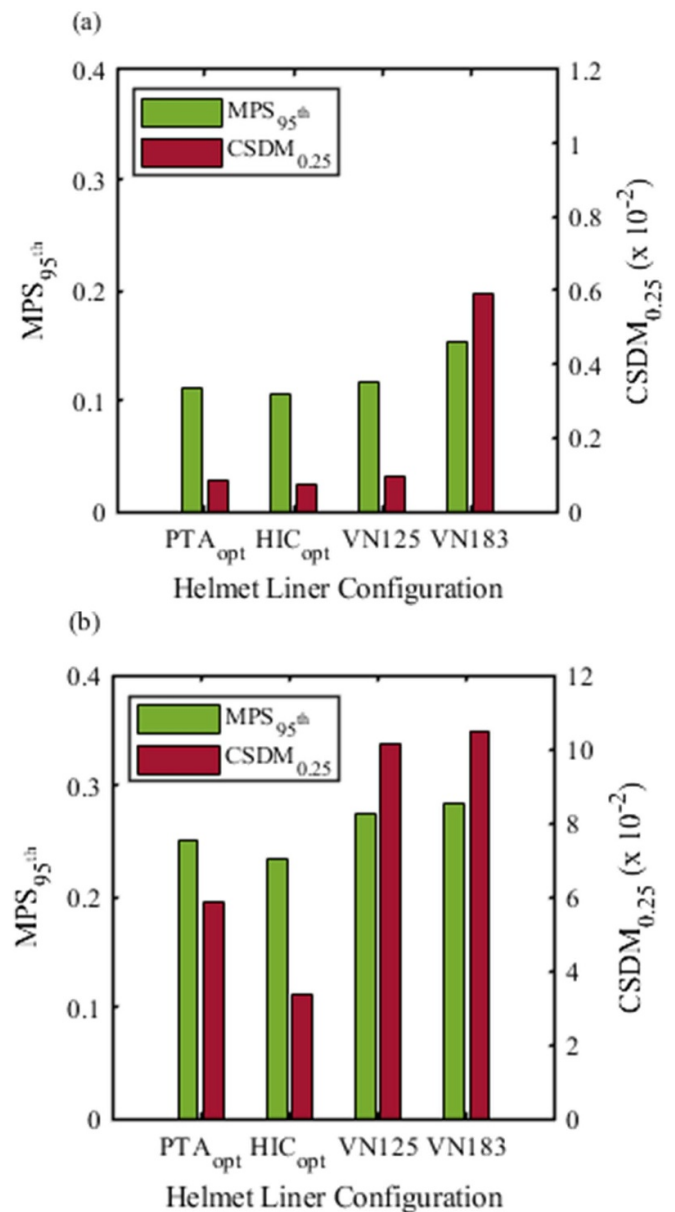
Figure 13. Comparison of tissue-based severity metrics, 95th percentile maximum principal strain and cumulative strain damage measure subject to (a) direct impact conditions and (b) oblique impact conditions.

0.112 and 0.106 respectively, representing a reduction of 3.4% and 8.6%. Similarly, the values for CSDM$_{0.25}$ reported for foam liner configurations exceed the values reported for the honeycomb liner configurations. For VN125 and VN183, the CSDM$_{0.25}$ was 0.000 97 and 0.0059 respectively. In comparison, the CSDM$_{0.25}$ for PTA$_{opt}$ and HIC$_{opt}$ were 0.000 87 and 0.000 74 respectively, representing a reduction of 10.3% and 23.7%.

Figure 13(b) reports the MPS$_{95th}$ and CSDM$_{0.25}$ for the oblique impact conditions reported in figure 11. The values of MPS$_{95th}$ reported for foam liner configurations exceed the values reported for the honeycomb liner configurations. For

VN125 and VN183, the MPS$_{95th}$ was 0.275 and 0.284 respectively. In comparison, the MPS$_{95th}$ for PTA$_{opt}$ and HIC$_{opt}$ were 0.252 and 0.234 respectively, representing a reduction of 8.4% and 14.9%. Similarly, the values for CSDM$_{0.25}$ reported for foam liner configurations exceed the values reported for the honey- comb liner configurations. For VN125 and VN183, the CSDM$_{0.25}$ was 0.105 and 0.102 respectively. In comparison, the CSDM$_{0.25}$ for PTA$_{opt}$ and HIC$_{opt}$ were 0.057 and 0.034 respectively, representing a reduction of 44.1% and 66.7%.

Figure 14(a) illustrates the distribution of MPS within the finite element brain model. It is important to note that the visualised data includes 100th percentile values. The contours demonstrate that the MPS developed is 0.35 and 0.44 for VN125 and VN183 respectively. In comparison, the distribution and concentration of MPS is less notable for PTA$_{opt}$ and HIC$_{opt}$ where the maximum values recorded were 0.33 and 0.30. Figure 14(b) illustrates the distribution of MPS within the finite element brain model. The contours demonstrate that the MPS developed is 0.50 and 0.54 for VN125 and VN183 respectively. In comparison, the distribution and concentration of MPS is less notable for PTA$_{opt}$ and HIC$_{opt}$ where the maximum values recorded were 0.43 and 0.40.

4. Discussion

The finite element-based optimisation procedure identified configurations of a pre-buckled structure that minimised peak translational acceleration and HIC. The results of the simulations show that adopting a liner composed of the optimised honeycomb structure can reduce the severity of impacts. The improvements observed are due to adopting a structure with high stiffness and densification strain, which can be optimised relative to specific boundary conditions (e.g. mass, velocity, and contact area). Elastomeric foams, as well as other foams, do not possess the geometric freedom to facilitate this degree of optimisation, hence cellular structures such as the pre-buckled honeycomb hold an advantage for this application. Moreover, foams absorb the energy of the impact due to crushing but fail to distribute the load laterally due to their negligible Poisson's ratio. Since the foam deforms in a concentrated area, despite its large deformation and significant local energy absorption, it cannot distribute the energy of the impact. In contrast, honeycomb type structures, as well as other cellular structures, can better distribute the energy of the impact by engaging a larger portion of the liner in large deformation and energy absorption [38].

When subject to oblique conditions, the honeycomb structures yielded a reduction in both translational and rotational acceleration. The ratio of out-of-plane stiffness to in-plane stiffness facilitates a helmet liner with a lower shear stiffness, whilst maintaining sufficient normal stiffness, such that the tangential force that gives rise to rotational acceleration is reduced [68]. Furthermore, in-plane collapse of the honeycomb cells aids the mitigation of translational acceleration. This is attributed to the transversely isotropic properties of
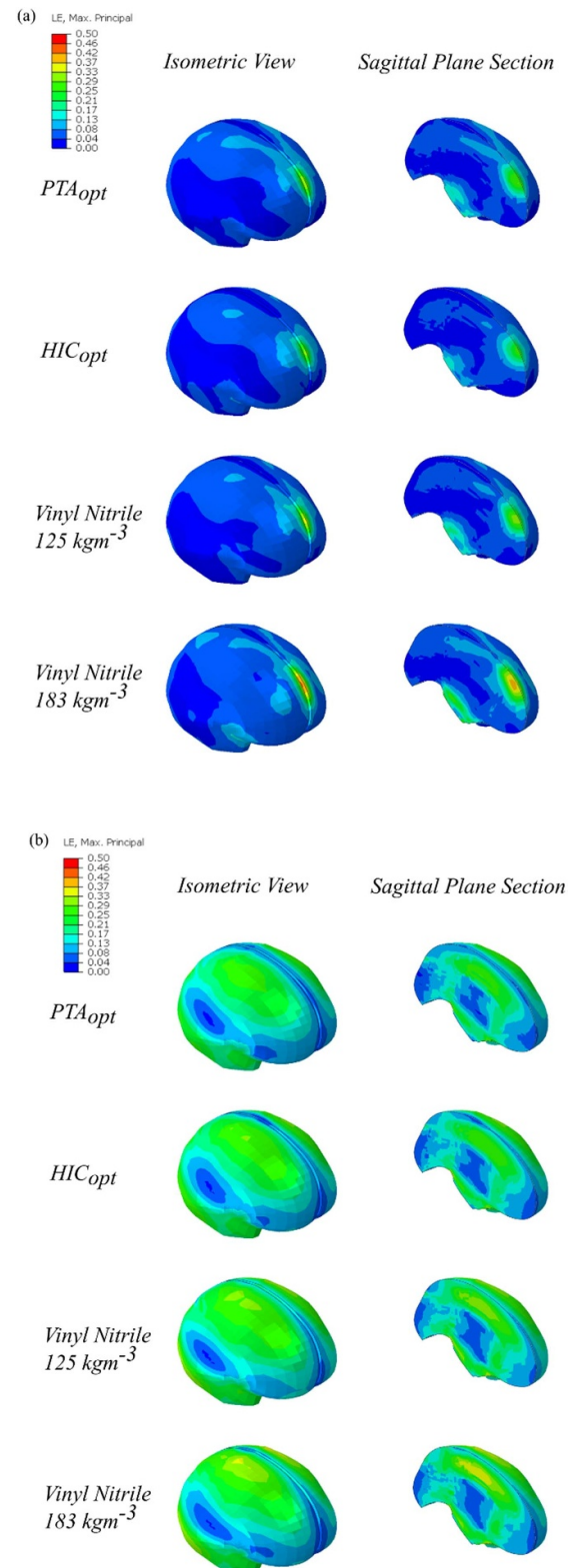

Figure 14. Comparison of maximum principal strain distribution within the finite element head model when subject to (a) direct impact conditions and (b) oblique impact conditions for honeycomb and foam helmet variants.

the pre-buckled honeycomb structure. Foams possess notably greater isotropic behaviour, hence the rotational acceleration reported was larger [24, 69].

Comparison between the results for the PBC model used in the optimisation strategy, and the full-scale helmet model, reported notable deviation in terms of PTA and HIC. Generally, the PBC model under-reports both the HIC ($r_d = 10.9\%$–20.9%) and PTA values ($r_d = 12.7\%$–35.2%). This is due to modelling discrepancies between the PBC model and full-scale helmet model. Firstly, the kinematics of the PBC model do not match that of the helmet model. In the PBC model, motion is restrained to exclusively translate in the Z axis, whilst in the helmet model the headform is unrestrained and is therefore free to translate and rotate. As such, the PBC model better represents the guided fall loading conditions of the American standards (e.g. ASTM) which include a rigid neck that restrains motion rather than the free fall conditions of the British and European standards [55, 70]. Secondly, the PBC model fails to account for the curvature of the headform and shell, instead adopting for a flat-on-flat impact. Whilst this was adopted as a modelling simplification, in a typical helmet impact, the area of the liner engaged during the impact increases with increasing strain, reaching a maximum at the point of densification. Hence, mechanical behaviour which adopts a flat plateau may not be appropriate for helmet designs. As such, the optimal performance, based on the flat-on-flat performance, does not translate to the in-situ helmet loading conditions. This suggests that whilst foams are considered to have ideal energy absorption behaviour, they fail to show these characteristics for impact loading. Lastly, the PBC model does not account for the inclusion of the shell. The polymeric shell serves to distribute the load under impact and behaves differently to the rigid plates used in the optimisation. This modelling decision assumes an infinitely rigid shell, thus facilitating overly effective load distribution. In reality, the shell deforms away from the impact site and pushes the liner from the impact site. Future studies should refine this limitation to improve the predictive capacity of the optimisation procedure.

The results demonstrated that the pre-buckled honeycomb liners reduced the kinematic-based injury metrics when compared to the elastomeric foam liners. Kinematic-based injury metrics, however, fail to account for different material and morphological details of the brain anatomy. Hence, established tissue-based metrics, 95th percentile MPS and CSDM were calculated using a finite element model of the head. Further analysis demonstrated that both MPS_{95th} and $CSDM_{0.25}$ were reduced for impacts including the pre-buckled honeycomb liners. For direct impact conditions, marginal decreases in MPS_{95th} and $CSDM_{0.25}$ were observed. In contrast, for oblique conditions, notable reductions were observed. This is because the main mechanism of development of strain in the brain and ultimately brain injury, is rotational kinematics [10].

The mass of the helmet liner is an important design constraint in the development of helmet liners. Previous work has shown that a 20% increase in the mass of the head-helmet assembly can decrease the head acceleration by 10% [71]. Further analysis has identified that there is in fact an inverse relationship between peak head acceleration and the
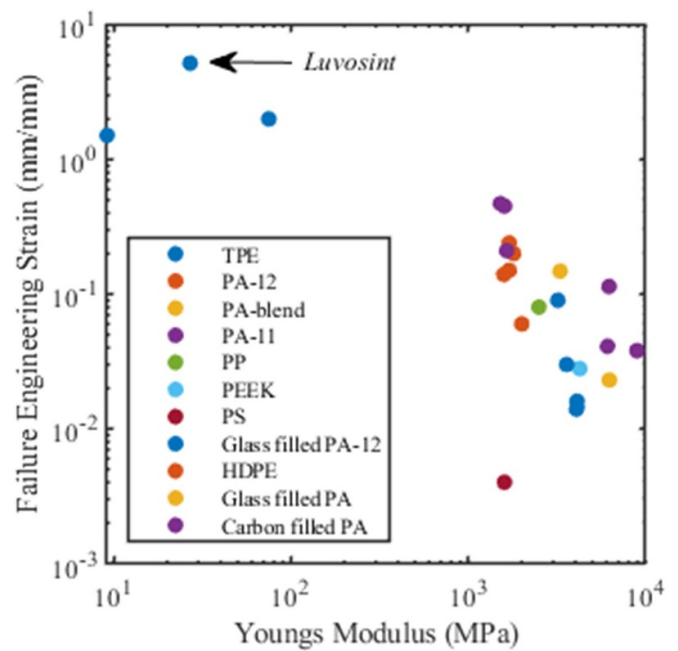
Figure 15. Distribution of material properties relative to elongation and Youngs modulus for laser sintered polymers.

square root of mass [72]. Adopting designs with increased mass, however, is not an appropriate design strategy as this ultimately leads to user discomfort. The reported density for the PTA_{opt} and HIC_{opt} configurations were 277 kgm^{-3} and 198 kgm^{-3}, representing an increase in mass of 51.3% and 8.1%, respectively. Considering the inverse square law previously discussed, these increases in mass yield a reduction in peak accelerations of 7.2% and 2.8%. As the reported reductions in translational and rotational acceleration were notably greater, it can be concluded that the benefit was driven by the structure and not the addition of mass. The optimised configurations satisfied the design standard performance threshold and exceeded the performance of materials currently used in helmets, meaning that the adopted base material is a limiting factor in the design. Adopting alternative elastomers that exhibit increased stiffness, as reported by figure 15, would maintain the desirable recoverable mechanical properties but would allow use of thinner walls, enabling weight reduction whilst retaining performance.

This study is limited by the simplified model used to inform the optimisation, as it did not capture the influence of shell geometry and stiffness, nor did it consider other helmet functional requirements that are application specific—for example crush, or penetration resistance [73]. Furthermore, certification tests are conducted under multiple orientations, various temperatures conditions as well as against kerbstone anvils [74]. Further refinement would be required before this method can be used to effectively identify new material structures for helmet liner design and certification. Despite this, the study represents the first efforts to identify a complete method for finite element-based optimisation of material structures for

helmet liners which has been verified using tissue-based severity metrics informed by a finite element head model.

5. Conclusions

In this paper, we provide an investigation into the performance of an elastomeric pre-buckled honeycomb structure design, informed through a finite element-based optimisation strategy for use in helmet liners. Comparison was drawn relative to a traditional foam liner, VN. The pre-buckled honeycomb liner can outperform traditional liners under both direct and oblique impact conditions. The geometric freedom of this structure enables a transversely isotropic behaviour—which affords more effective mitigation of rotational acceleration, whilst the variable out-of-plane behaviour enables optimised mitigation of translational acceleration. Consequently, both kinematic and tissue-based metrics injury metrics are reduced. The optimisation strategy, based on a simplified PBC model, is scalable to the full behaviour of the helmet system. The reported approach has shown promise to optimise material structures for future helmet designs.
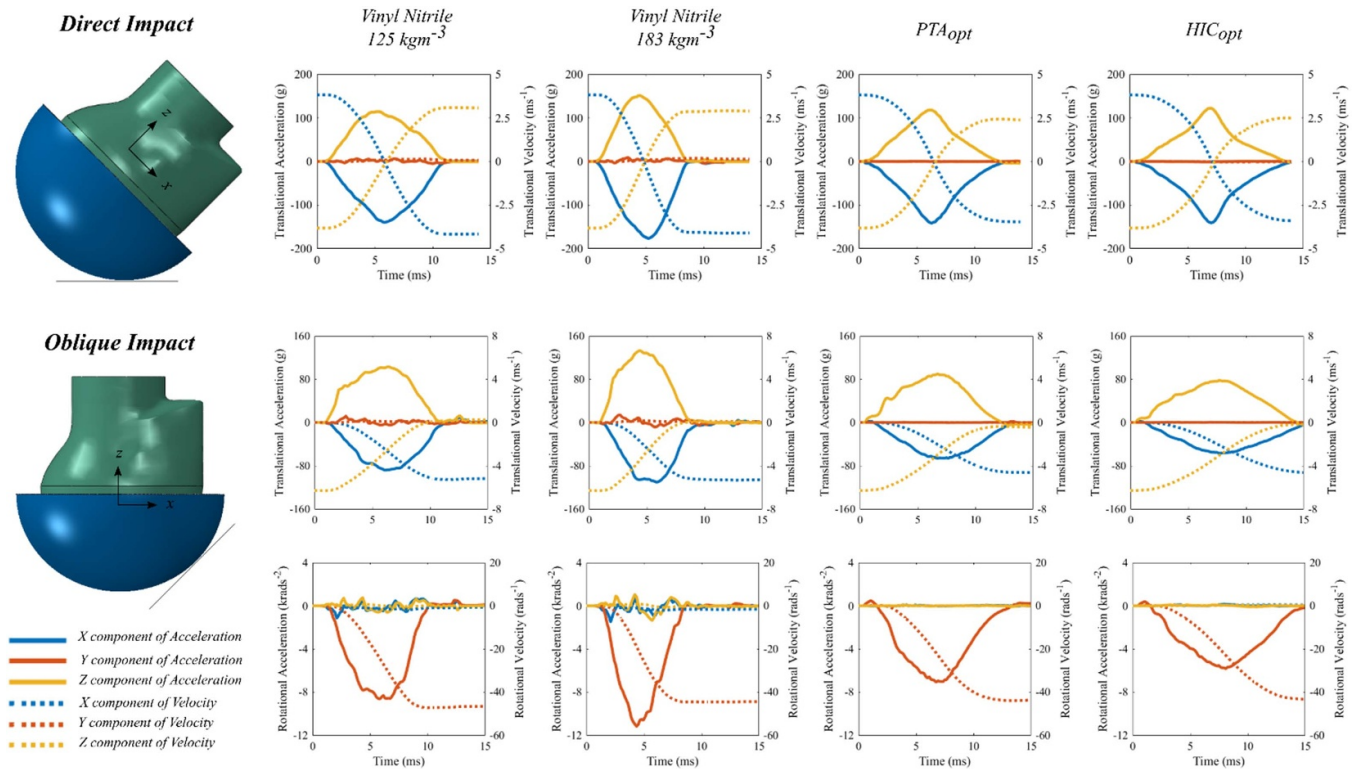
Data availability statement

All data that support the findings of this study are included within the article (and any supplementary files).

Appendix

Figure A1. All recorded kinematic data, translational and rotational acceleration, and velocity, for helmet liner materials, Vinyl Nitrile 125 kgm^{-3}, Vinyl Nitrile 125 kgm^{-3}, Honeycomb variants PTA$_{opt}$ and HIC$_{opt}$ under direct and oblique impact conditions.

ORCID iDs

Rhosslyn Adams ⓘ https://orcid.org/0000-0001-5098-5328
Shwe Soe ⓘ https://orcid.org/0000-0001-7621-0344
Peter Theobald ⓘ https://orcid.org/0000-0002-3227-7130

References

[1] Roebuck-Spencer T and Cernich A 2014 Epidemiology and societal impact of traumatic brain injury *Handbook on the Neuropsychology of Traumatic Brain Injury* (Springer) pp 3–23

[2] Weber C D, Horst K, Lefering R, Hofman M, Dienstknecht T and Pape H-C 2016 Major trauma in winter sports: an international trauma database analysis *Eur. J. Trauma Emerg. Surg.* **42** 741–7

[3] Mueller B A, Cummings P, Rivara F P, Brooks M A and Terasaki R D 2008 Injuries of the head, face, and neck in relation to ski helmet use *Epidemiology* **19** 270–6

[4] Graves J M, Whitehill J M, Stream J O, Vavilala M S and Rivara F P 2013 Emergency department reported head injuries from skiing and snowboarding among children and adolescents, 1996–2010 *Inj. Prev.* **19** 399–404

[5] Rughani A I, Lin C-T, Ares W J, Cushing D A, Horgan M A, Tranmer B I, Jewell R P and Florman J E 2011 Helmet use and reduction in skull fractures in skiers and snowboarders admitted to the hospital *J. Neurosurg. Pediatr.* **7** 268–71

[6] Connor T A, Clark J M, Jayamohan J, Stewart M, McGoldrick A, Williams C, Seemungal B M, Smith R, Burek R and Gilchrist M D 2019 Do equestrian helmets prevent concussion? A retrospective analysis of head injuries and helmet damage from real-world equestrian accidents *Sports Med. Open* **5** 1–8

[7] King A I, Ruan J S, Zhou C, Hardy W N and Khalil T B 2009 Recent advances in biomechanics of brain injury research: a review *J. Neurotrauma* **12** 651–8

[8] Bradshaw D R S and Morfey C L 2001 Pressure and shear responses in brain injury models *SAE Technical Paper*

[9] Kleiven S 2013 Why most traumatic brain injuries are not caused by linear acceleration but skull fractures are *Front. Bioeng. Biotechnol.* **1** 15

[10] Holbourn A H S 1943 Mechanics of head injuries *Lancet* **242** 438–41

[11] Li S and Li Q M 2022 Head responses subjected to frontal translational acceleration loads *Int. J. Mech. Sci.* **231** 107598

[12] Tierney G 2021 Concussion biomechanics, head acceleration exposure and brain injury criteria in sport: a review *Sports Biomech.* 1–29

[13] Abderezaei J, Rezayaraghi F, Kain B, Menichetti A and Kurt M 2021 An overview of the effectiveness of bicycle helmet designs in impact testing *Front. Bioeng. Biotechnol.* **9** 1–13

[14] Wei W, Petit Y, Arnoux P J and Bailly N Head-ground impact conditions and helmet performance in E-scooter falls *Accid. Anal. Prev.* **181** 106935

[15] Post A, Oeur A, Hoshizaki B and Gilchrist M D 2013 Examination of the relationship between peak linear and angular accelerations to brain deformation metrics in hockey helmet impacts *Comput. Methods Biomech. Biomed. Eng.* **16** 511–9

[16] Adanty K, Clark J M, Post A, Hoshizaki T B and Gilchrist M D 2019 Comparing two proposed protocols to test the oblique response of cycling helmets to fall impacts *Int. J. Crashworthiness* **25** 648–63

[17] Post A, Oeur A, Hoshizaki B and Gilchrist M D 2013 An examination of American football helmets using brain deformation metrics associated with concussion *Mater. Des.* **45** 653–62

[18] Post A, Hashim E, Hoshizaki T B, Gilchrist M D and Cusimano M D 2021 A preliminary examination of the relationship between biomechanical measures and structural changes in the brain *Trauma* **23** 24–32

[19] Doorly M C and Gilchrist M D 2006 The use of accident reconstruction for the analysis of traumatic brain injury due to head impacts arising from falls *Comput. Methods Biomech. Biomed. Eng.* **9** 371–7

[20] Bland M L, McNally C, Zuby D S, Mueller B C and Rowson S 2020 Development of the STAR evaluation system for assessing bicycle helmet protective performance *Ann. Biomed. Eng.* **48** 47–57

[21] DiGiacomo G, Tsai S and Bottlang M 2021 Impact performance comparison of advanced snow sport helmets with dedicated rotation-damping systems *Ann. Biomed. Eng.* **49** 2805–13

[22] Gibson L J and Ashby M F 2014 *Cellular Solids: Structure and Properties* 2nd edn (Cambridge University Press)

[23] Gimbel G M and Hoshizaki T B 2008 Compressive properties of helmet materials subjected to dynamic impact loading of various energies *Eur. J. Sport Sci.* **8** 341–9

[24] Bailly N, Petit Y, Desrosier J-M, Laperriere O, Langlois S and Wagnac E 2020 Strain rate dependent behavior of vinyl nitrile helmet foam in compression and combined compression and shear *Appl. Sci.* **10** 8286

[25] Newman J A 2007 *Modern Sports Helmets: Their History, Science, and Art* (Schiffer Pub)

[26] Mosleh Y, Vander Sloten J, Depreitere B and Ivens J 2017 Novel composite foam concept for head protection in oblique impacts *Adv. Eng. Mater.* **19** 1700059

[27] Mosleh Y, Cajka M, Depreitere B, Vander Sloten J and Ivens J 2018 Designing safer composite helmets to reduce rotational accelerations during oblique impacts *Proc. Inst. Mech. Eng.* H **232** 479–91

[28] Vanden Bosche K, Mosleh Y, Depreitere B, Vander Sloten J, Verpoest I and Ivens J 2017 Anisotropic polyethersulfone foam for bicycle helmet liners to reduce rotational acceleration during oblique impact *Proc. Inst. Mech. Eng.* H **231** 851–61

[29] Dymek M, Ptak M and Fernandes F A O 2021 Design and virtual testing of American football helmets–a review *Arch. Comput. Methods Eng.* **29** 1–13

[30] Decker W, Baker A, Ye X, Brown P, Stitzel J and Gayzik F S 2020 Development and multi-scale validation of a finite element football helmet model *Ann. Biomed. Eng.* **48** 258–70

[31] Aare M and Kleiven S 2007 Evaluation of head response to ballistic helmet impacts using the finite element method *Int. J. Impact Eng.* **34** 596–608

[32] Pelanconi M and Ortona A 2020 Review on the design approaches of cellular architectures produced by additive manufacturing *Int. Conf. on Additive Manufacturing in Products and Applications* pp 52–64

[33] Raykar S J, Narke M M, Desai S B and Warke S S 2020 Manufacturing of 3D printed sports helmet *Techno-Societal 2018* (Springer) pp 771–8

[34] Nasim M, Hasan M J and Galvanetto U 2022 Impact behavior of energy absorbing helmet liners with PA12 lattice structures: a computational study *Int. J. Mech. Sci.* **233** 107673

[35] Hanna B, Adams R, Townsend S, Robinson M, Soe S, Stewart M, Burek R and Theobald P 2021 Auxetic metamaterial optimisation for head impact mitigation in American football *Int. J. Impact Eng.* **157** 103991

[36] Soe S P, Martin P, Jones M, Robinson M and Theobald P 2015 Feasibility of optimising bicycle helmet design safety through the use of additive manufactured TPE cellular structures *Int. J. Adv. Manuf. Technol.* **79** 1975–82

[37] Khosroshahi S F, Tsampas S A and Galvanetto U 2018 Feasibility study on the use of a hierarchical lattice architecture for helmet liners *Mater. Today Commun.* **14** 312–23

[38] Khosroshahi S F, Duckworth H, Galvanetto U and Ghajari M 2019 The effects of topology and relative density of lattice liners on traumatic brain injury mitigation *J. Biomech.* **97** 109376

[39] Clough E C, Plaisted T A, Eckel Z C, Cante K, Hundley J M and Schaedler T A 2019 Elastomeric microlattice impact attenuators *Matter* **1** 1519–31

[40] Bitzer T N 1997 *Honeycomb Technology: Materials, Design, Manufacturing, Applications and Testing* (Springer Science & Business Media)

[41] Li S, Xiao Z, Zhang Y and Li Q M 2021 Impact analysis of a honeycomb-filled motorcycle helmet based on coupled head-helmet modelling *Int. J. Mech. Sci.* **199** 106406

[42] Caserta G D, Iannucci L and Galvanetto U 2011 Shock absorption performance of a motorbike helmet with honeycomb reinforced liner *Compos. Struct.* **93** 2748–59

[43] Bliven E, Bourdet N, Deck C and Madey S M 2019 A novel strategy for mitigation of oblique impacts in bicycle helmets forensic biomechanics *Artic. J. Forensic Biomech.* **10** 1

[44] Bland M L, Zuby D S, Mueller B C and Rowson S 2018 Differences in the protective capabilities of bicycle helmets in real-world and standard-specified impact scenarios *Traffic Inj. Prev.* **19** S158–S163

[45] Hansen K, Dau N, Feist F, Deck C, Willinger R, Madey S M and Bottlang M 2013 Angular impact mitigation system for bicycle helmets to reduce head acceleration and risk of traumatic brain injury *Accid. Anal. Prev.* **59** 109–17

[46] Bhudolia S K, Gohel G and Leong K F 2020 Enhanced energy absorption characteristics of novel integrated hybrid honeycomb/polystyrene foam *J. Cell. Plast.* **57** 839–48

[47] Abayazid F F, Carpanen D and Ghajari M 2022 New viscoelastic circular cell honeycombs for controlling shear and compressive responses in oblique impacts *Int. J. Mech. Sci.* **222** 107262

[48] Robinson M *et al* 2019 Mechanical characterisation of additively manufactured elastomeric structures for variable strain rate applications *Addit. Manuf.* **27** 398–407

[49] Townsend S, Adams R, Robinson M, Hanna B and Theobald P 2020 3D printed origami honeycombs with tailored out-of-plane energy absorption behavior *Mater. Des.* **195** 108930

[50] Adams R, Townsend S, Soe S and Theobald P 2022 Mechanical behaviour of additively manufactured elastomeric pre-buckled honeycombs under quasi-static and impact loading *Mater. Des.* **213** 110368

[51] Adams R, Townsend S, Soe S and Theobald P 2021 Finite element-based optimisation of an elastomeric honeycomb for impact mitigation in helmet liners *Int. J. Mech. Sci.* **214** 106920

[52] Ramirez B J, Kingstedt O T, Crum R, Gamez C and Gupta V 2017 Tailoring the rate-sensitivity of low density polyurea foams through cell wall aperture size *J. Appl. Phys.* **121** 225107

[53] Adams R, Soe S P, Santiago R, Robinson M, Hanna B, McShane G, Alves M, Burek R and Theobald P 2019 A novel pathway for efficient characterisation of additively

manufactured thermoplastic elastomers *Mater. Des.*
180 107917

[54] BS EN 960 2006 *Headforms for use in the testing of protective helmets* (https://doi.org/10.3403/19976887)

[55] Whyte T, Stuart C A, Mallory A, Ghajari M, Plant D J, Siegmund G P and Cripton P A 2019 A review of impact testing methods for headgear in sports: considerations for improved prevention of head injury through research and standards *J. Biomech. Eng.* **141** 444–6

[56] Shuaeib F M, Hamouda A M S, Hamdan M M, Radin Umar R S and Hashmi M S J 2002 Motorcycle helmet: part II. Materials and design issues *J. Mater. Process. Technol.* **123** 422–31

[57] Connor T A, Stewart M, Burek R and Gilchrist M D 2019 Influence of headform mass and inertia on the response to oblique impacts *Int. J. Crashworthiness* **24** 677–98

[58] Sandberg M, Tse K M, Bin Tan L and Lee H P 2018 A computational study of the EN 1078 impact test for bicycle helmets using a realistic subject-specific finite element head model *Comput. Methods Biomech. Biomed. Eng.* **21** 684–92

[59] Mills N J and Gilchrist A 2006 Bicycle helmet design *Proc. Inst. Mech. Eng.* L **220** 167–80

[60] Trotta A, Clark J M, McGoldrick A, Gilchrist M D and Annaidh A N 2020 Biofidelic finite element modelling of brain trauma: importance of the scalp in simulating head impact *Int. J. Mech. Sci.* **173** 105448

[61] Johnson K L, Chowdhury S, Lawrimore W B, Mao Y, Mehmani A, Prabhu R, Rush G A and Horstemeyer M F 2016 Constrained topological optimization of a football helmet facemask based on brain response *Mater. Des.* **111** 108–18

[62] User C A E 2014 *ABAQUS 6.14 Analysis User Guide* (Dassault Systèmes)

[63] Abayazid F, Ding K, Zimmerman K, Stigson H and Ghajari M 2021 A new assessment of bicycle helmets: the brain injury mitigation effects of new technologies in oblique impacts *Ann. Biomed. Eng.* **49** 2716–33

[64] Versace J 1971 A review of the severity index *SAE Technical Papers* (https://doi.org/10.4271/710881)

[65] Kimpara H, Nakahira Y, Iwamoto M, Rowson S and Duma S 2011 Head injury prediction methods based on 6 degree of freedom head acceleration measurements during impact *Int. J. Automot. Eng.* **2** 13–19

[66] Horgan T J and Gilchrist M D 2003 The creation of three-dimensional finite element models for simulating head impact biomechanics *Int. J. Crashworthiness* **8** 353–66

[67] Horgan T J and Gilchrist M D 2004 Influence of Fe model variability in predicting brain motion and intracranial pressure changes in head impact simulations *Int. J. Crashworthiness* **9** 401–18

[68] Abram D E, Wikarna A, Golnaraghi F and Wang G G 2020 A modular impact diverting mechanism for football helmets *J. Biomech.* **99** 109502

[69] Ling C, Ivens J, Cardiff P and Gilchrist M D 2018 Deformation response of EPS foam under combined compression-shear loading. Part II: high strain rate dynamic tests *Int. J. Mech. Sci.* **145** 9–23

[70] Meng S, Cernicchi A, Kleiven S and Halldin P 2019 The biomechanical differences of shock absorption test methods in the US and European helmet standards *Int. J. Crashworthiness* **24** 399–412

[71] Ghajari M, Peldschus S, Galvanetto U and Iannucci L 2011 Evaluation of the effective mass of the body for helmet impacts *Int. J. Crashworthiness* **16** 621–31

[72] Siegkas P, Sharp D J and Ghajari M 2019 The traumatic brain injury mitigation effects of a new viscoelastic add-on liner *Sci. Rep.* **9** 1–10

[73] Soe S, Robinson M, Giasin K, Adams R, Palkowski T and Theobald P 2021 Using FFF and topology optimisation to increase crushing strength in equestrian helmets BT *Sustainable Design and Manufacturing 2020* pp 369–77

[74] Connor T A *et al* 2016 Current standards for sports and automotive helmets: a review *Ref. Ares* **3151745** 1–42